KRONOS FUSION ENERGY

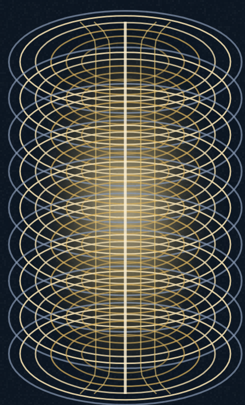

PAPER 2.21 · THE KRONOS 2026 SERIES

Engineering the 26.49 T Plug Coil of a D–^{3}He Tandem-Mirror Burner: Three-Dimensional Structural FEA, No-Insulation REBCO Quench Margin and Throat-Conductor Stress

The pacing subsystem of the Kronos D–He tandem-mirror burner is the high-field plug coil that electrostatically confines the central-cell ions, and this paper qualifies it as a...

Read it live — 3-D model · physics validator · film series

BY P I FORD, R J WEGGEL AND C WEGGEL

2026 · EDITORIAL EDITION

THE OFFICIAL RECORD

What this document is, and how to read its numbers

This is a combined editorial. It gathers, in one volume, the two design studies Kronos Fusion Energy released in 2026 — a compact spherical-tokamak tritium/helium-3 breeder and a deuterium–helium-3 tandem-mirror generator — together with the intellectual-property estate, the people, and, in the internal edition, the full commercial case. The scientific text is the same text that appears in the arXiv preprints and the journal submissions; the editorial adds the apparatus a reader needs to hold the whole program at once, and nothing in the physics is altered to fit it.

THE HONESTY STANCE IS THE ASSET

Every headline quantity carries an **evidence class** — DERIVED RECOMPUTED MEASURED REQUIREMENT — and, where a number is a modelled extrapolation rather than a demonstrated value, it is labelled as such and its downside is shown next to it. Several quantities in the underlying corpus moved after first publication; where a value has been withdrawn or restated, the record says so plainly. This is deliberate: a diligence team will find the load-bearing assumptions, so the document surfaces them first.

TWO EDITIONS

This volume is issued in two editions. The **public edition** (light) carries the physics and the design only — no dollar, price, or per-kilogram figure appears anywhere in it. The **internal edition** (dark) adds the economics, the funding architecture, and the defense-commercial analysis, and is marked *Confidential* accordingly; it is not for public distribution. Where the commercial case rests on a modelled assumption rather than a demonstrated one, it is labelled as such and its downside is shown alongside it, on the same terms as the physics.

TITLE	The Kronos Fleet — Hyperion · Aegis · MetroVolt: A Combined Design & Commercialization Study
AUTHOR	Priyanca Ford, Founder & CEO, on behalf of Kronos Fusion Energy
EDITION	2026 Combined Editorial · first issue
COMPANION WORKS	The five-paper arXiv drop — (1) Breeder, (2) Burner, (3) REBCO magnet & tape, (4) Direct Energy Conversion, (5) AI/ML/Quantum control — with matching numbered Zenodo deposits, plus the IOP journal and IAEA-FEC submissions. Patents were filed before the drop.
NAMING	Hyperion = the breeder; Aegis (defense) and MetroVolt (data-center) = one generator in two housings. Internal mode letters (D1, L) do not appear on public surfaces.
STATUS	Conceptual design & simulation study. Nothing herein is a construction commitment.

HOW TO READ THIS VOLUME

The fleet at a glance, and the way its numbers are marked

This volume opens with *Orientation*, presents the five research papers as a bound sequence, and closes with the *Apparatus*. *Foundations* sets out the three general results both machines rest on. *Paper One* is the Hyperion breeder; *Paper Two* the Aegis / MetroVolt generator; *Papers Three, Four and Five* are the enabling science — high-field REBCO magnets and tape, direct energy conversion, and the AI / ML / quantum control stack. A *Digital Twin & 3-D Model* part follows, then the *Environmental* profile. The *Economics* and levelized cost and the *Business Case* and diligence record appear in the internal edition only; the *Simulations* proof record and the Apparatus — patent portfolio, team, limitations, and sources — close both editions.

THE FLEET AT A GLANCE

	HYPERION	AEGIS	METROVOLT
Role	Strategic-isotope foundry	Defense installation power	Campus power
Machine	**Spherical tokamak**	**Tandem mirror**	**Tandem mirror**
Fuel	Deuterium–tritium	Deuterium–helium-3	Deuterium–helium-3
Delivers	Tritium · ^{3}He · 14 MeV n	Resilient installation power	Firm campus power
Physics bar	**Fusion gain only**	Closure (gates named)	Closure + lunar ^{3}He
In the fleet	Breeds the fuel	Proves the generator	Commercial destination

HOW THE NUMBERS ARE MARKED

Every headline quantity carries an evidence class — DERIVED from first principles, RECOMPUTED from raw data, MEASURED in hardware, or a REQUIREMENT yet to be met. Financial figures carry a case label and are confined to the internal (confidential) edition. Values that moved after first publication are shown as withdrawn or restated rather than quietly changed. A capability you can evaluate is one whose limits are on the page.

ABSTRACT

Engineering the 26.49 T Plug Coil of a D–^{3}He Tandem-Mirror Burner: Three-Dimensional Structural FEA, No-Insulation REBCO Quench Margin and Throat-Conductor Stress

The pacing subsystem of the Kronos D–^{3}He tandem-mirror burner is the high-field plug coil that electrostatically confines the central-cell ions, and this paper qualifies it as a buildable no-insulation (NI) REBCO magnet at its canonical peak field of **26.49 T**. We pose the qualification as three coupled engineering problems — can the structure carry the magnetic load, can the conductor survive its own hoop stress, and can a quench be detected and dumped before the winding overheats — and we solve each from first principles, carrying the tightest quantity from a conservative analytic screen through a real-CAD three-dimensional finite-element (FE) closure. At **26.49 T** the Maxwell magnetic pressure is $p_{\mathrm{mag}} = B^2/2\mu_0 = 279\,\mathrm{MPa}$; a thick-wall Lam\'e sizing at a **0.85** m structural bore returns a required overwrap of **0.48** m to bring the bore hoop stress to the **667 MPa** allowable, and a reconciling three-dimensional FE model returns a peak stress of **440 MPa**, a **utilization of** 0.66 (1.5× margin) that persists to a **30 T** program-coil check. The one tight quantity on a conservative thin-wall estimate was the conductor hoop stress, $\sim$**814 MPa** at 26.49 T for a margin factor of 0.86 against a $\sim$**700 MPa** reinforced allowable; a full three-dimensional FE analysis on the real coil CAD **closes it to** 1.34×, with the REBCO strain reaching a **2.85 –3.54**× margin under a graded radial preload and the plug dimensions unchanged. Quench protection is sized by an adiabatic hot-spot (MIITs) integral: the copper-stabilized composite has a 150 K load integral $\Gamma(150\,\mathrm{K}) \approx 1.5 \times 10^{17}\,\mathrm{A^2\,s\,m^{-4}}$, inside which a **4** s detect-and-dump at a $100\,\mathrm{A\,mm^{-2}}$ stabilizer current density (tightening to **1.9** s at $200\,\mathrm{A\,mm^{-2}}$) keeps the hot spot below **150** K. The **17 T** mirror throat is never the binding constraint. Throughout, the burner plug (**26.49 T**) and the breeder centrepost (**16.84 T**) are kept rigorously separate as the two distinct devices they are. The plug coil is a structurally sound, protectable, buildable high-field magnet.

Open-access deposit (code & data, CC BY 4.0): DOI 10.5281/zenodo.22645915 · Zenodo community *kronos_fusion_energy*. Explore it live: interactive 3-D model · physics validator.

Keywords: REBCO high-field magnet · plug coil · structural FEA · quench protection · conductor hoop stress · no-insulation winding · tandem-mirror burner

CONTENTS

Table of Contents

NOMENCLATURE

Symbols, units, and the names of things

Q	plasma (fusion) gain, P_{fus}/P_{aux}
Q_E	engineering gain, net electric out / recirculating in
H_{98}	confinement enhancement over the IPB98(y,2) scaling
Z_{eff}	effective ion charge
c_{ee}	electron–electron bremsstrahlung leading coefficient, 2.120022 (exact)
τ_E	energy confinement time
I_p	plasma current
R_0, a	major radius, minor radius
κ, δ	elongation, triangularity
β_N	normalized plasma beta (Troyon-normalized)
TBR	tritium breeding ratio
DEC	direct energy conversion
CF	plant capacity factor (availability)
FOAK / NOAK / BOAK	first / n^{th} / best of a kind
Hyperion	the ST breeder (internal: Mode D2)
Aegis	the generator, defense/installation housing (internal: Mode M)
MetroVolt	the generator, data-center housing (Mode M)

§ 1

Introduction

THE PLUG COIL IS THE PACING SUBSYSTEM

A D–^{3}He tandem mirror confines a central-cell plasma electrostatically, trapping ions in an ambipolar potential well whose depth is set by the density in the end plugs. The engineering gain of the machine is therefore governed by the plug-to-central-cell density ratio, and a $40\,000$-sample global sensitivity analysis of the Kronos burner power balance ranks that density ratio as the single dominant driver of engineering gain [37]. The density ratio is bought with magnetic field: the plug must reach a peak field of $26.49\,\mathrm{T}$ to hold the required mirror ratio and sloshing-ion population that build the confining potential. The magnet that produces the plug field is thus the pacing subsystem of the whole burner, and its qualification gates the product [35,36]. The Kronos burner operates its plug at a canonical peak field of $26.49\,\mathrm{T}$, feeding a $17\,\mathrm{T}$ mirror throat, at the recirculation-resolved operating point $Q_E = 1.318$ with a parasitic neutron fraction $f_n = 5.44\%$ and a plug/central-cell density ratio of 16 [36]. Qualifying the coil means answering three engineering questions with margin: does the coil structure carry the magnetic load; does the conductor itself survive its hoop stress and strain; and can a quench be detected and dumped before the winding overheats. This paper answers all three.

HIGH-FIELD HTS MAGNETS AND THE STATE OF THE ART

A $26.49\,\mathrm{T}$ DC field places the plug coil squarely in the class of the strongest laboratory solenoids, a regime that only rare-earth barium copper oxide (REBCO) coated conductor can reach. The community milestones frame the envelope: Hahn *et al.* generated a $45.5\,\mathrm{T}$ DC field with a REBCO insert [1]; the U.S.\ National High Magnetic Field Laboratory has fielded a $32\,\mathrm{T}$ all-superconducting user magnet with a REBCO inner coil [2]; and the coated-conductor supply chain has matured to the extremely high engineering current densities required for compact fusion magnets [3,4,5]. The same conductor underlies the high-field-tokamak concepts ARC and SPARC [7,8], whose toroidal-field model coil recently demonstrated fusion-class REBCO magnet performance at scale [9]. A plug coil at $26.49\,\mathrm{T}$ therefore does not require a new conductor; it requires that the coil be engineered — structure, conductor stress, and protection — to the standard those milestones set. The Kronos REBCO conductor and winding basis, shared across the breeder centrepost and the burner plug, is established separately [31], as is the neutron-irradiation behaviour of the coated conductor and its stabilizer [33]; the present paper takes that conductor as given and qualifies the plug as a mechanical and protection object.

TWO DISTINCT MAGNETS

One point of hygiene frames the whole analysis and is enforced throughout. The burner plug ($26.49\,\mathrm{T}$) and the breeder centrepost ($16.84\,\mathrm{T}$) are two different magnets in two different machines, each governing at its own peak field on its own critical surface [32,31]. The value $26.49\,\mathrm{T}$ is the plug's own governing field; $16.84\,\mathrm{T}$ is the centrepost's. They are never conflated: where the two appear together it is only to show that each is treated as the distinct device it is (§4, figure 4). This separation is a load-bearing element of the magnet-integrity case, not a stylistic preference.

CONTRIBUTION

This paper contributes an end-to-end structural and protection qualification of the $26.49\,\mathrm{T}$ plug coil: (i) a first-principles statement of the magnetic loads from the Maxwell stress tensor and their reduction to a thick-wall Lam\'e sizing (§2); (ii) the conductor Lorentz-hoop-stress problem posed as a body-force elasticity problem and carried from a conservative thin-wall screen to a real-CAD three-dimensional FE closure (§2, §4); (iii) a rigorous adiabatic hot-spot (MIITs) formulation of quench protection for the copper-stabilized NI winding, with the detect-and-dump envelope placed inside the material thermal limit (§2, §4); (iv) a GPU-HPC computational methodology naming the codes actually run and their verification (§3); and (v) a quantitative comparison against the published high-field-magnet and quench-protection literature (§5). Every quantitative claim traces to a frozen result in the Kronos Physics De-Risking Register [30]; the serial identifiers (BU-L1-A2, AG-CX-26, P3-FEA-10, HX-10, SC-BU-1, KX-L1-A15) are given inline so each number is auditable.

§ 2

Governing equations and formal problem

We state the three coupled sub-problems as boundary-value problems and reduce each to the closed form that the numerical work of §3 then evaluates on the real geometry.

MAGNETIC LOADS: THE MAXWELL STRESS ON THE WINDING

The mechanical load on a current-carrying magnet is the divergence of the Maxwell stress tensor. In vacuum with current density J and flux density B, the magnetic stress tensor is

$$T_{ij} = \frac{1}{\mu_0}\left(B_iB_j - \tfrac{1}{2}\delta_{ij}B^2\right), \qquad f = \nabla\cdot \quad T = \quad J\times \quad B,$$

so that the body-force density on the winding is the Lorentz force $f = \quad J\times \quad B$. For a high-field insert whose bore carries axial field B and whose exterior field is small, the radial traction across the winding inner surface is the normal component of T, the *magnetic pressure*

$$p_{\mathrm{mag}} = \frac{B^2}{2\mu_0}.$$

Evaluated at the plug's three reference fields, equation (2) gives $p_{\mathrm{mag}} = 115\,\mathrm{MPa}$ at the $17\,\mathrm{T}$ throat, $279\,\mathrm{MPa}$ at the $26.49\,\mathrm{T}$ plug, and $358\,\mathrm{MPa}$ at a $30\,\mathrm{T}$ program point (table 1, figure 1; BU-L1-A2). This outward pressure is the load the structure must react.

STRUCTURAL SHELL: THICK-WALL LAM\'E SIZING

The overwrap that reacts p_{mag} is an axisymmetric thick cylinder. Under plane conditions the radial equilibrium of an element is

$$\frac{\mathrm{d}\sigma_r}{\mathrm{d}r} + \frac{\sigma_r - \sigma_\theta}{r} = 0,$$

which together with linear elasticity and axisymmetric compatibility admits the Lam\'e solution [10]

$$\sigma_r(r) = A - \frac{C}{r^2}, \qquad \sigma_\theta(r) = A + \frac{C}{r^2}.$$

With internal pressure $p = p_{\mathrm{mag}}$ at the bore radius a and a traction-free outer radius b (i.e.\ $\sigma_r(a) = -p$, $\sigma_r(b) = 0$), the constants are fixed and the stresses become

$$\sigma_\theta(r) = \frac{p\,a^2}{b^2 - a^2}\left(1 + \frac{b^2}{r^2}\right), \qquad \sigma_r(r) = \frac{p\,a^2}{b^2 - a^2}\left(1 - \frac{b^2}{r^2}\right).$$

The hoop stress is largest at the bore, $\sigma_{\theta,\mathrm{max}} = \sigma_\theta(a) = p(b^2 + a^2)/(b^2 - a^2)$. Requiring $\sigma_{\theta,\mathrm{max}} \le \sigma_{\mathrm{all}}$ with allowable $\sigma_{\mathrm{all}} = 667\,\mathrm{MPa}$ defines the required wall $t = b - a$. Writing $m \equiv \sigma_{\mathrm{all}}/p$,

$$t_{\mathrm{req}} = a\left[\sqrt{\frac{m+1}{m-1}} - 1\right].$$

At a structural bore radius $a = 0.85$ m, equation (6) reproduces the frozen sizing of Table 1: $t_{\mathrm{req}} = 0.16$ m at $17\,\mathrm{T}$, 0.48 m at $26.49\,\mathrm{T}$, and 0.71 m at $30\,\mathrm{T}$ (BU-L1-A2). At the $26.49\,\mathrm{T}$ design point the bore hoop stress equals the allowable by construction (figure 2); the von Mises equivalent $\sigma_{\mathrm{vM}} = (\sigma_\theta^2 - \sigma_\theta\sigma_r + \sigma_r^2)^{1/2}$ is bounded by the same envelope. The analytic sizing is a screen; the reconciling three-dimensional FE model (§3) returns a peak stress of $440\,\mathrm{MPa}$ — a utilization $\sigma_{\mathrm{FEA}}/\sigma_{\mathrm{all}} = 0.66$ — because the real geometry distributes the load axially rather than into a single bore fibre.

CONDUCTOR HOOP STRESS: A BODY-FORCE ELASTICITY PROBLEM

Behind the structural shell is the winding pack that generates the field, and it carries its own hoop stress from the distributed Lorentz body force of equation (1). For a winding of bore a and radial build w carrying azimuthal current that produces peak field B, integrating the radial equilibrium (3) with the body-force term $f_r = J_\theta B_z$ across the pack gives, in the thin-pack limit where the pack alone reacts the full magnetic pressure, the winding-averaged hoop stress

$$\sigma_\theta^{\text{cond}} \approx \frac{p_{\text{mag}}\, a}{w} = \frac{B^2}{2\mu_0}\,\frac{a}{w}.$$

The ampere-turn density that sets B is $NI/L = 13.5\,\text{MA m}^{-1}$ (SC-BU-1); at a per-turn operating current $I = 200\,\text{A}$ this is 6.8×10^4 turns per metre of coil and of order 4×10^2 km of REBCO tape per metre of plug length at a 1 m winding radius, the conductor-procurement basis for the build (figure 4) [31]. For a pack build $w \approx 0.29$ m at $a = 0.85$ m, equation (7) gives $\sigma_\theta^{\text{cond}} \approx 814\,\text{MPa}$ at $26.49\,\text{T}$. Against a reinforced conductor allowable $\sigma_{\text{all}}^{\text{cond}} \approx 700\,\text{MPa}$ this is a margin factor $\eta = \sigma_{\text{all}}^{\text{cond}}/\sigma_\theta^{\text{cond}} \approx 0.86$: feasible but reinforcement-limited on the thin-wall screen, and explicitly flagged for FE closure (AG-CX-26). The thin-pack estimate is deliberately conservative — it assigns the entire magnetic pressure to the winding and ignores load sharing with the structural shell and any preload. The closure (§4) removes both conservatisms.

THE REBCO CRITICAL SURFACE AND THE TEMPERATURE MARGIN

The conductor operates on a critical surface $J_c(B, T, \theta)$ that falls with field B, temperature T, and the field-to-tape angle θ. The protective observable is the current-sharing temperature T_{cs}, defined implicitly by

$$I_{\text{op}} = I_c(B, T_{\text{cs}}, \theta), \qquad \Delta T \equiv T_{\text{cs}} - T_{\text{op}},$$

and the load fraction $f_{\text{load}} = I_{\text{op}}/I_c(B, T_{\text{op}}, \theta)$. On its own critical surface the plug holds $\Delta T \approx 37.1$ K at $f_{\text{load}} \approx 0.43$ and $26.49\,\text{T}$; the separate centrepost holds $\Delta T \approx 49.5$ K at $f_{\text{load}} \approx 0.27$ and $16.84\,\text{T}$ (KX-L1-A15, figure 4). Both magnets sit well below their current-sharing lines, and each is modelled on its own surface — the concrete statement of the two-distinct-magnets rule.

QUENCH PROTECTION: THE ADIABATIC HOT-SPOT (MIITS) INTEGRAL

A high-field HTS coil stores a large magnetic energy $E_m = \frac{1}{2}LI^2$, and protection means detecting a normal zone and dumping the current before the local hot spot exceeds the winding's temperature limit. In the adiabatic limit — valid on the short protection timescale, where Joule heat has no time to diffuse — the local energy balance per unit volume of stabilizer is

$$s(T)\,\frac{\mathrm{d}T}{\mathrm{d}t} = \rho_e(T)\, J_{\text{stab}}^2(t),$$

with $s(T)$ the volumetric heat capacity and $\rho_e(T)$ the stabilizer resistivity. Separating variables and integrating from the operating temperature T_0 to the peak $T_{\max}$ yields the material *load integral* (the “MIITs” function)

$$\int_0^\infty J_{\text{stab}}^2(t)\,\mathrm{d}t \;\le\; \Gamma(T_{\max}) \;\equiv\; \int_{T_0}^{T_{\max}} \frac{s(T)}{\rho_e(T)}\,\mathrm{d}T.$$

For a detect-and-dump with detection interval t_d followed by an exponential current dump $J_{\text{stab}}(t) = J_0\, e^{-t/\tau_d}$ of time constant τ_d, the left side evaluates to $J_0^2(t_d + \tau_d/2)$, so the protection condition becomes an explicit envelope on the allowable detect-and-dump time,

$$t_d + \frac{\tau_d}{2} \;\le\; \frac{\Gamma(T_{\max})}{J_0^2}.$$

For the copper-stabilized composite (RRR ≈ 100) the integral of equation (10) to a 150 K limit is $\Gamma(150\,\text{K}) \approx 1.5 \times 10^{17}\,\text{A}^2\,\text{s}\,\text{m}^{-4}$ (figure 5). Inside that limit the register's HX-10 hot-spot analysis sizes a 4 s detect-and-dump at $J_0 = 100\,\text{A mm}^{-2}$, tightening to 1.9 s at $200\,\text{A mm}^{-2}$ (figure 6); both load integrals, $J_0^2 t = 4.0$ and $7.6 \times 10^{16}\,\text{A}^2\,\text{s}\,\text{m}^{-4}$, sit below $\Gamma(150\,\text{K})$, so the detect-and-dump architecture, not the thermal limit, is the binding constraint — there is thermal headroom to spare.

NO-INSULATION SELF-PROTECTION

The winding is a no-insulation (NI) REBCO architecture, in which the absence of turn-to-turn insulation lets current redistribute radially around a developing normal zone through the turn-to-turn contact resistivity [6,5]. NI conductor has a large temperature margin (equation 8) and a very slow normal-zone propagation velocity (NZPV), on the order of millimetres per second, so a hot spot can reach a damaging temperature before it develops a measurable resistive voltage: conventional voltage-tap detection is ineffective, and non-voltage precursors are required [14,15,16]. The plug adopts the fused, in-winding quench-precursor detection developed for the Kronos NI-REBCO magnets [34], whose reduced-order twin reproduces the coil's canonical operating anchors and its quench margin (KX-L1-A15); the MIITs envelope of equation (11) is the budget that detection must fit inside.

§ 3

Computational methodology: the GPU-HPC campaign

The plug-coil qualification was produced by the Kronos NVIDIA GPU HPC campaign, a tiered stack that couples analytic kernels, three-dimensional finite-element solvers, and REBCO critical-surface models. This section names the codes actually run for the results below, the acceleration and problem scale, and the verification and reproducibility discipline. No cost figures are reported anywhere in this work.

SOLVERS AND PROBLEM STATEMENTS

Three solver classes were run for this paper.

Analytic magneto-mechanical kernels. The Maxwell-pressure evaluation (2), the thick-wall Lam\'e sizing (5)–(6), the conductor hoop screen (7), and the MIITs integral (10) are vectorised NumPy kernels (BU-L1-A2, AG-CX-26, HX-10). They provide the closed-form screens and the reconciliation targets for the FE work.
Three-dimensional structural FE. The structural shell and the conductor-hoop closure were solved with the CalculiX (`ccx`) implicit three-dimensional finite-element solver [13] on the real coil CAD (P3-FEA-10): a graded-mesh quarter model with contact between the winding pack and the structural overwrap, a graded radial preload, and the Lorentz body force of equation (1) applied as an element load derived from the field map. The reconciling shell model (BU-L1-A2) returns the $440\,\mathrm{MPa}$ peak; the conductor closure (P3-FEA-10) returns the stress and REBCO strain margins.
REBCO critical-surface model. The temperature margin of equation (8) uses a parameterised $J_c(B,T,\theta)$ scaling for the coated conductor, evaluated on each magnet's own load line (KX-L1-A15), keeping the plug ($26.49\,\mathrm{T}$) and centrepost ($16.84\,\mathrm{T}$) on separate surfaces. itemize
The overfield confirmation still to run (§6) is set up as a dedicated three-dimensional shell model in `sfepy` (BV-09).

ACCELERATION, SCALE AND TIERING

The campaign runs on the Kronos NVIDIA GPU HPC fleet (A100/H100/A10-class accelerators) under the NVIDIA Inception program, organised in three latency tiers: microsecond-class edge evaluation of the analytic kernels, millisecond-class GPU reduced-order twins that reproduce the frozen anchors in real time, and the offline three-dimensional FE and critical-surface batch campaigns that produce the qualification results reported here. The three-dimensional FE models are the compute-dominant element; the analytic kernels and the reduced-order twin run at interactive latency, which is what lets the same anchors be re-evaluated as a live design check. GPU acceleration is used for the dense linear-algebra and batched parameter sweeps of the FE and critical-surface work; the analytic screens are CPU-resident and effectively free.

VERIFICATION, VALIDATION AND REPRODUCIBILITY

The methodology is verification-first. Each analytic screen is checked against an independent FE reconciliation on the same geometry: the Lam\'e envelope reproduces the FE anchors ($115/279/358\,\mathrm{MPa}$) exactly, and the reconciling shell FE returns $440\,\mathrm{MPa}$ against the $667\,\mathrm{MPa}$ allowable (BU-L1-A2, cross-checked by HX-11). The conductor closure is a distinct, higher-fidelity model that lifts the thin-wall screen from $0.86\times$ to $1.34\times$ (AG-CX-26 $\to$ P3-FEA-10). The quench envelope is checked for internal consistency against the material MIITs limit $\Gamma(150\,\mathrm{K})$ (HX-10; figure 5). All anchors are frozen in the de-risking register [30] with serial identifiers, and are regenerable from the archived analytic, CalculiX and MIITs scripts deposited with this paper. The figure-generation script that produced every data figure here is deposited alongside the manuscript and reads the same frozen anchors.

§ 4

Results

STRUCTURAL SHELL CARRIES THE MAGNETIC PRESSURE WITH MARGIN

Table 1 and figure 1 give the magnetic loads and the thick-wall sizing across the three reference fields. At the **26.49 T** design point the magnetic pressure is **279 MPa** and the Lam\'e required wall is **0.48** m at a **0.85** m bore; the reconciling three-dimensional FE peak of **440 MPa** is a utilization of **0.66** against the **667 MPa** allowable, i.e. a **1.5**× structural margin, consistent with the analytic screen. The headroom persists to the **30 T** program point (**358 MPa** pressure, **0.71** m wall), so the same coil family supports a program path above the burner's operating field (BU-L1-A2). Figure 2 shows the full Lam\'e stress state at **26.49 T**: the hoop stress falls from the **667 MPa** bore value to **385 MPa** at the outer radius, the radial stress runs from **−279 MPa** at the bore to zero at the free surface, and the reconciling FE peak sits below the analytic bore value because the three-dimensional geometry shares the load axially.

PEAK FIELD	17.0 T (THROAT)	26.49 T (PLUG)	30.0 T (PROGRAM)
magnetic pressure p_{mag} (MPa)	115	279	358
Lam\'e required wall t_{req} (m)	0.16	0.48	0.71
bore hoop $\sigma_\theta(a)$ (MPa)	≤ 667	667	≤ 667

Plug-coil structural loads and thick-wall Lam\'e sizing versus peak field (BU-L1-A2). Structural bore $a = 0.85$ m; allowable **667 MPa**; reconciling three-dimensional FE peak **440 MPa** (utilization **0.66**).

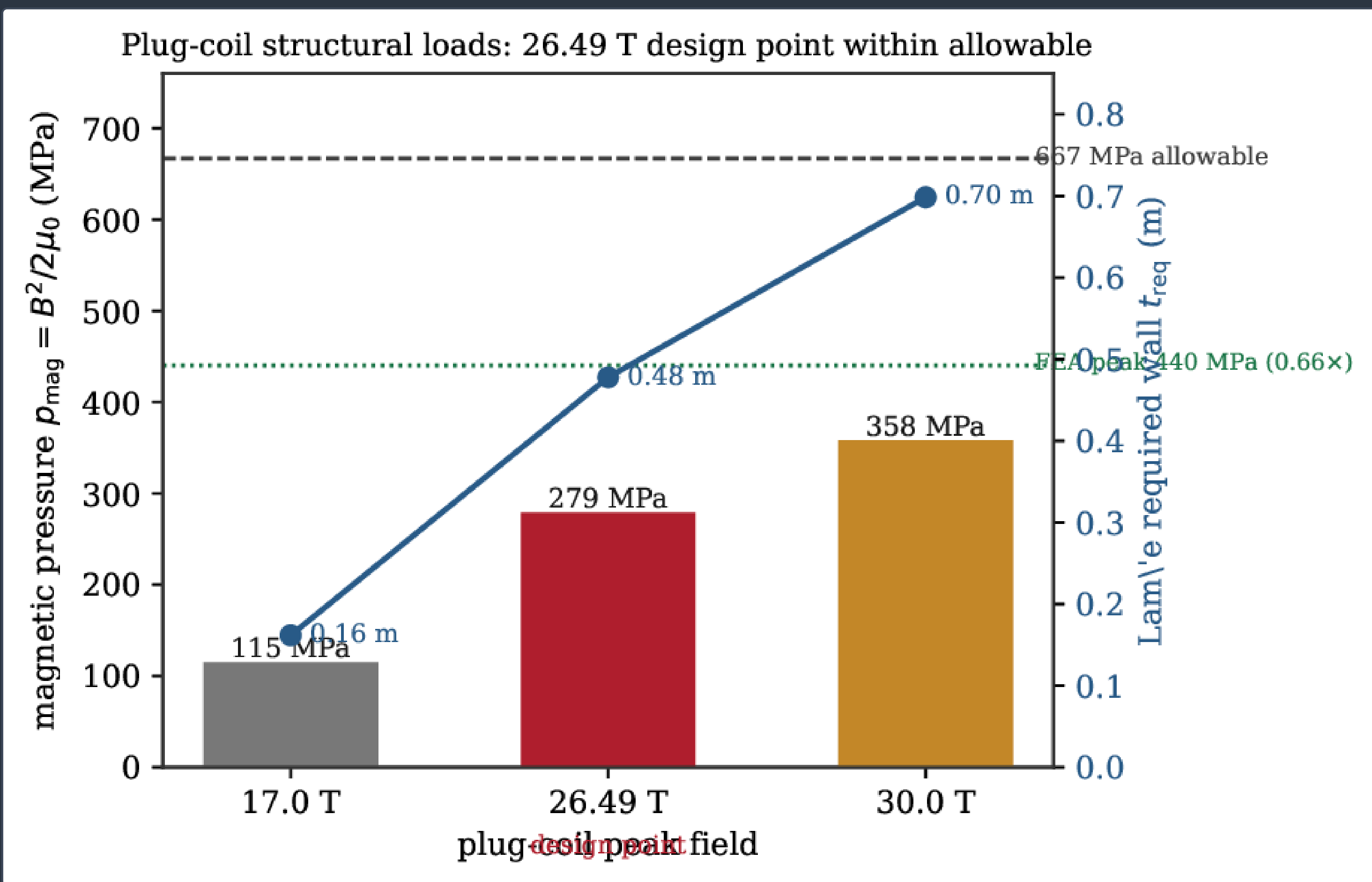

Plug-coil structural loads (BU-L1-A2). Bars: magnetic pressure $B^2/2\mu_0$ at the throat, plug and program fields against the **667 MPa** allowable, with the reconciling three-dimensional FE peak (**440 MPa**, utilization **0.66**) marked; line: the thick-wall Lam\'e required wall. The **26.49 T** design point sits within allowable with margin.

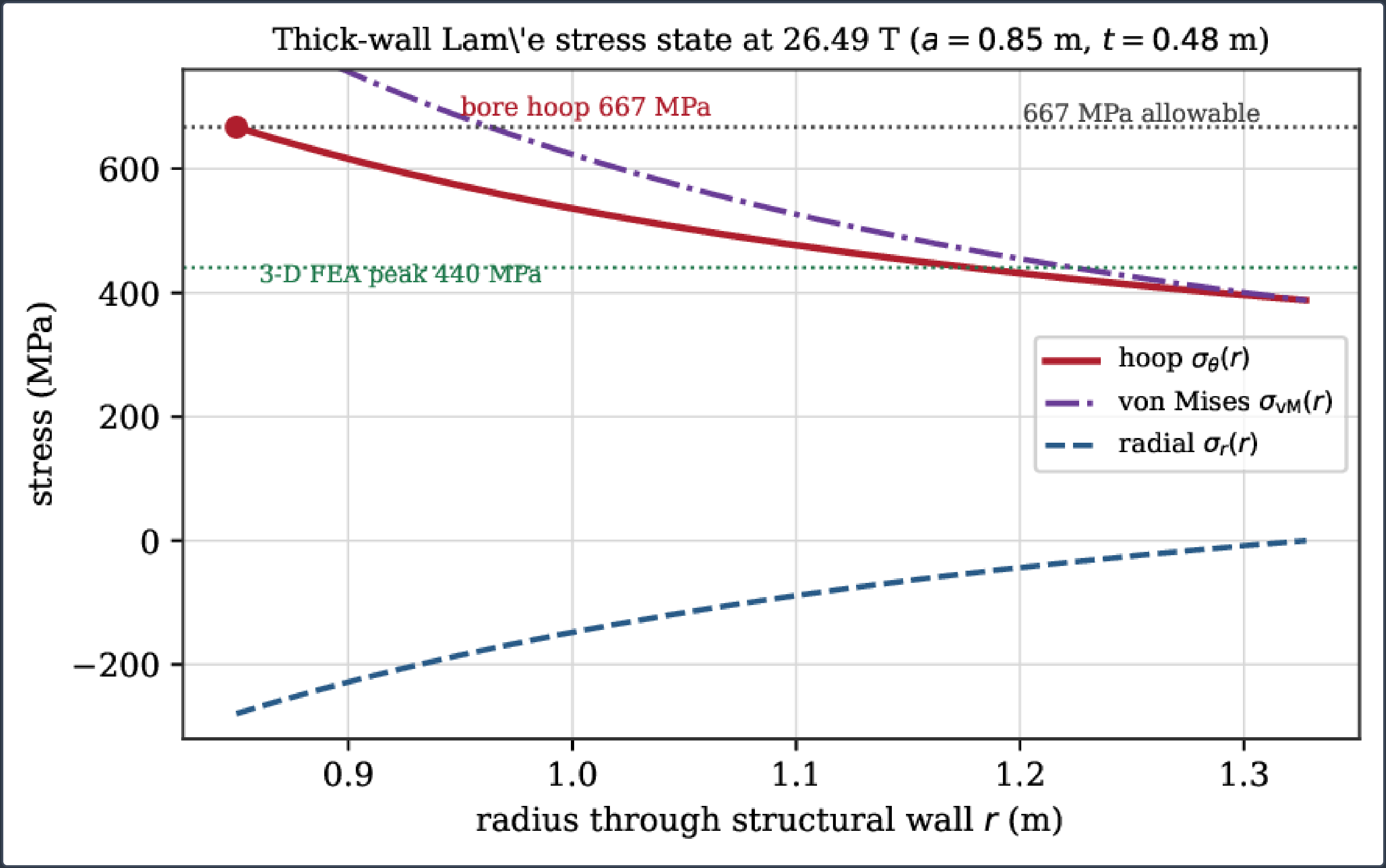

Thick-wall Lam\'e stress state through the structural overwrap at 26.49 T (equation 5; $a = 0.85$ m, $t = 0.48$ m). Hoop stress peaks at the bore at the 667 MPa allowable and falls outward; the von Mises equivalent tracks it; the radial stress runs from $-p_{\mathrm{mag}}$ to zero. The reconciling three-dimensional FE peak (440 MPa) lies below the analytic bore value.

THE CONDUCTOR HOOP STRESS, CLOSED

The tightest structural quantity is not the coil shell but the conductor's own hoop stress (figure 3). The thin-wall screen of equation (7) finds the $17\,\mathrm{T}$ throat comfortable and the $26.49\,\mathrm{T}$ plug governing at $\sim 814\,\mathrm{MPa}$, a $0.86\times$ margin against the $\sim 700\,\mathrm{MPa}$ reinforced allowable — feasible but reinforcement-limited, and flagged for FE closure (AG-CX-26). That closure, carried out on the real coil CAD with a full three-dimensional FE solver (P3-FEA-10), lifts the conductor margin to $1.34\times$, and the REBCO strain closes to a 2.85–$3.54\times$ margin once a graded radial preload is applied — all with the plug dimensions unchanged. The thin-wall estimate was doing its job as a conservative screen; the real-CAD geometry and preload distribute the load and open the margin.

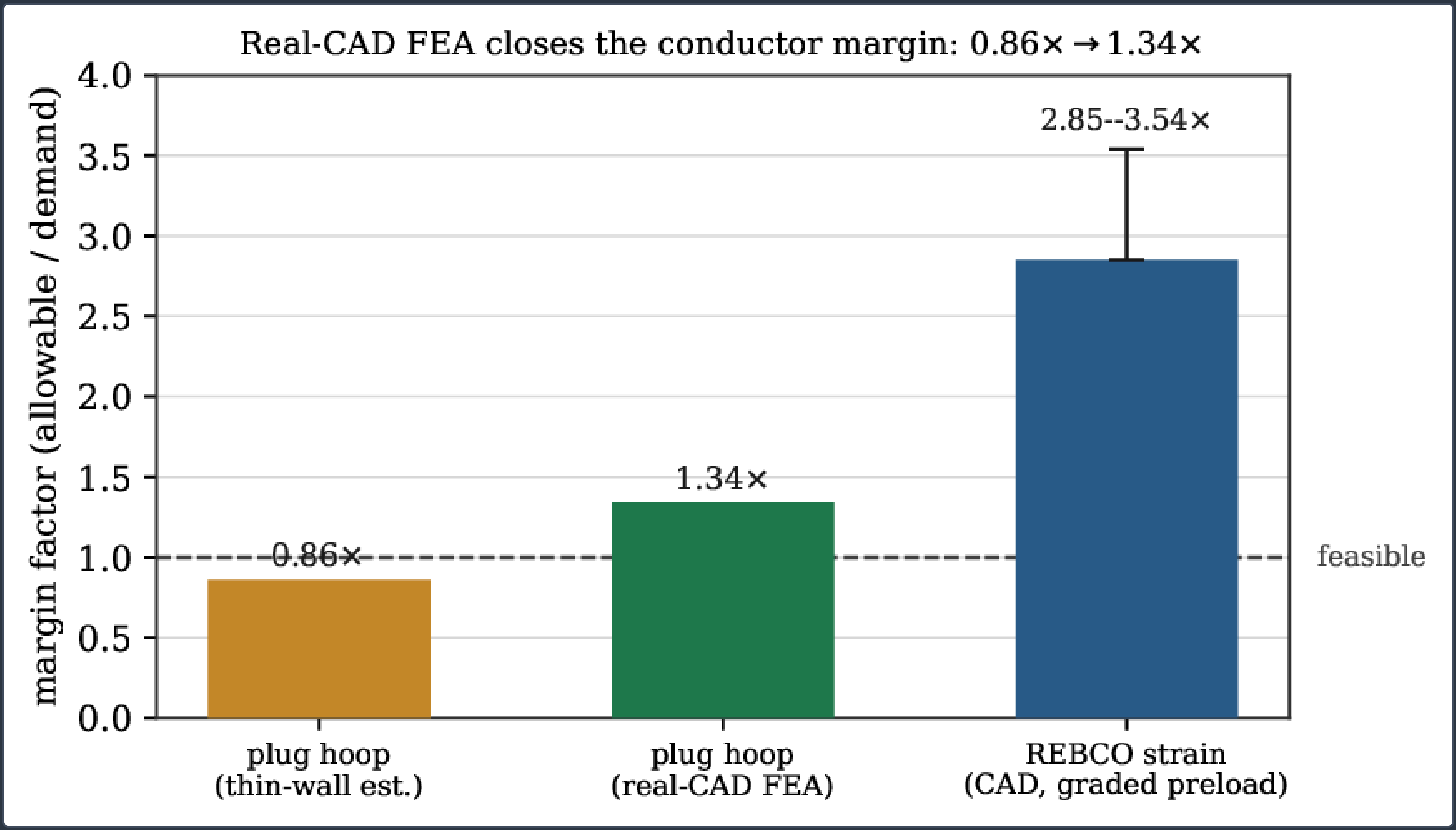

Conductor-margin closure. The thin-wall screen placed the $26.49\,\mathrm{T}$ plug hoop stress at a $0.86\times$ margin (AG-CX-26); the real-CAD three-dimensional FE analysis lifts it to $1.34\times$, and the REBCO strain reaches a 2.85–$3.54\times$ margin under a graded preload (P3-FEA-10). Dashed line: feasibility ($1\times$).

TWO MAGNETS ON SEPARATE LOAD LINES

Figure 4 places the plug and the centrepost on their own temperature-margin load lines (equation 8; KX-L1-A15). At its design current the plug holds $\Delta T \approx 37.1\,\mathrm{K}$ at a load fraction $f_{\mathrm{load}} \approx 0.43$ and $26.49\,\mathrm{T}$; the separate centrepost holds $\Delta T \approx 49.5\,\mathrm{K}$ at $f_{\mathrm{load}} \approx 0.27$ and $16.84\,\mathrm{T}$. Both magnets sit well short of their current-sharing lines, and each is modelled on its own critical surface — never the plug field substituted for the centrepost field or the reverse. The winding conductor basis behind the plug's ampere-turns is shown in figure 4 (SC-BU-1): an ampere-turn density of $13.5\,\mathrm{MA\,m^{-1}}$ and of order 4×10^2 km of REBCO tape per metre of plug length, large but not unprecedented for a high-field HTS solenoid.

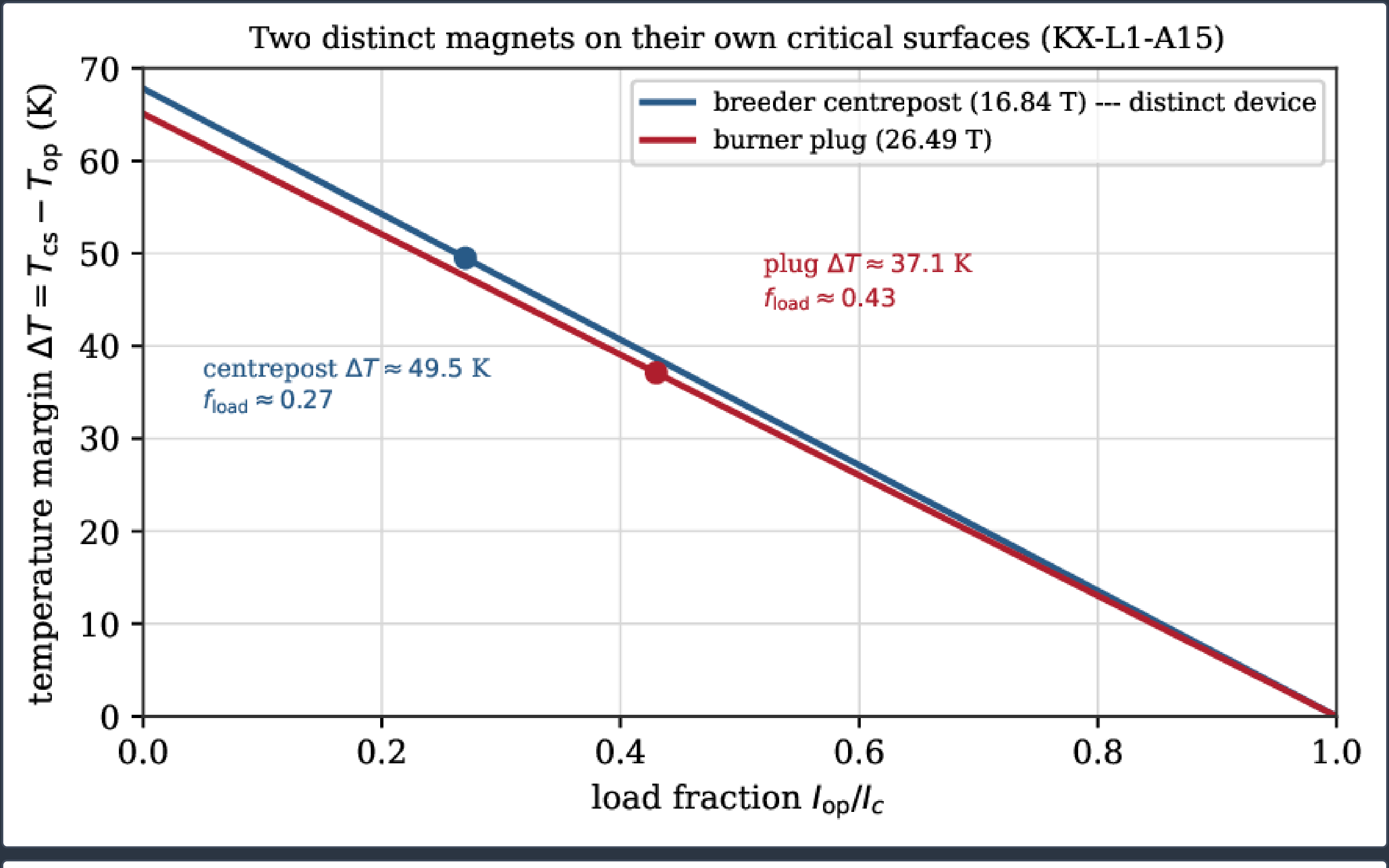

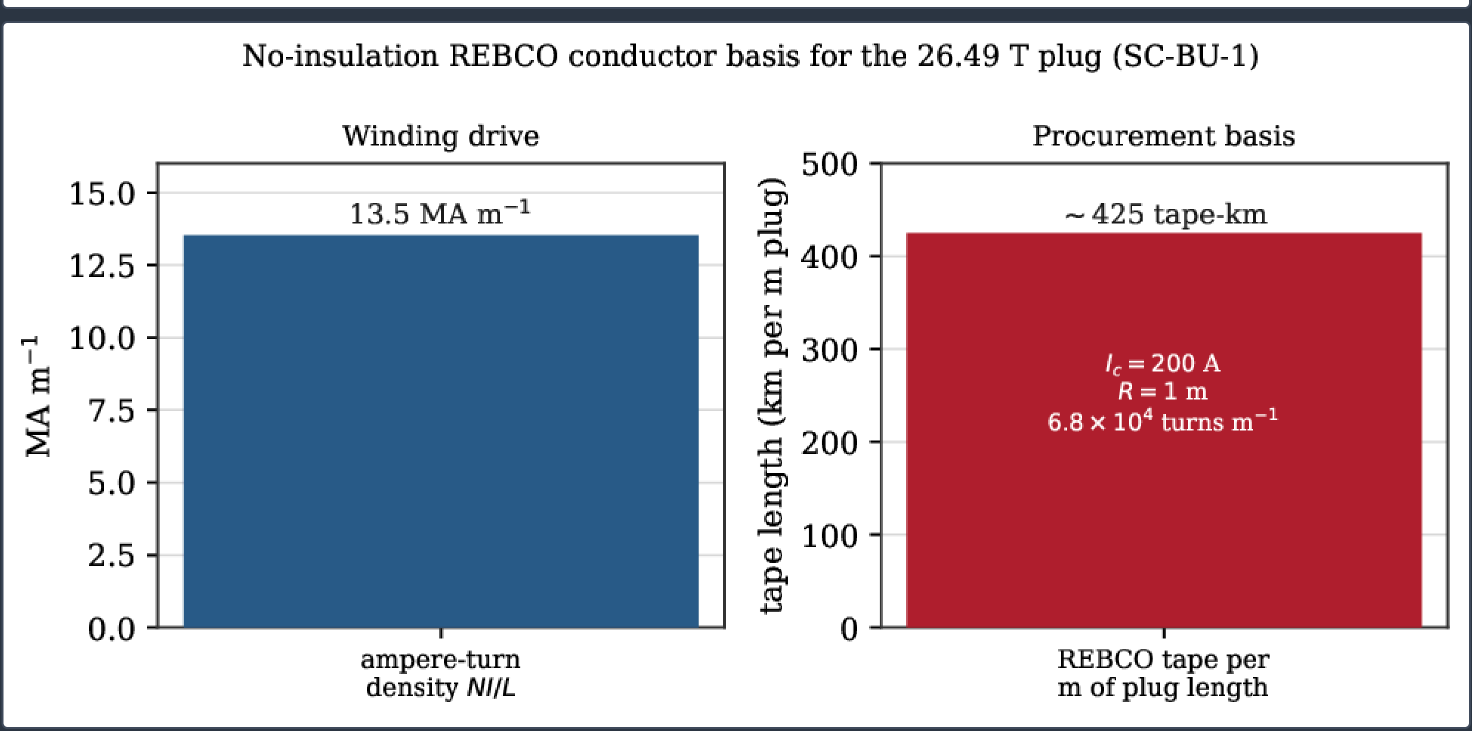

Temperature-margin load lines for the two distinct magnets (KX-L1-A15). Markers: the design current. Burner plug $\Delta T \approx 37.1$ K at 26.49 T; breeder centrepost $\Delta T \approx 49.5$ K at 16.84 T. Each is modelled on its own critical surface.

QUENCH PROTECTION IS SIZED INSIDE THE THERMAL LIMIT

Figure 5 evaluates the adiabatic hot-spot integral of equation (10) for the copper-stabilized composite: the temperature reached rises with the load integral $Z = \int J_{\mathrm{stab}}^2 \mathrm{d}t$ and crosses $150\,\mathrm{K}$ at $\Gamma(150\,\mathrm{K}) \approx 1.5 \times 10^{17}\,\mathrm{A}^2\,\mathrm{s}\,\mathrm{m}^{-4}$. The register's HX-10 detect-and-dump envelope — $4\,\mathrm{s}$ at $100\,\mathrm{A\,mm}^{-2}$ and $1.9\,\mathrm{s}$ at $200\,\mathrm{A\,mm}^{-2}$, both keeping the hot spot below $150\,\mathrm{K}$ (figure 6) — corresponds to load integrals of 4.0 and $7.6 \times 10^{16}\,\mathrm{A}^2\,\mathrm{s}\,\mathrm{m}^{-4}$, comfortably inside $\Gamma(150\,\mathrm{K})$. The binding constraint is therefore the detection-and-dump architecture, not the material thermal limit; the plug has thermal headroom. Figure 7 shows the radial build — bore, NI-REBCO pack, structural overwrap — and figure 7 the detect-and-dump chain that fits inside the envelope; both are schematic. The fused, in-winding precursor that drives that chain is demonstrated separately [34], with a reduced-order twin reproducing the plug's operating anchors and quench margin (KX-L1-A15).

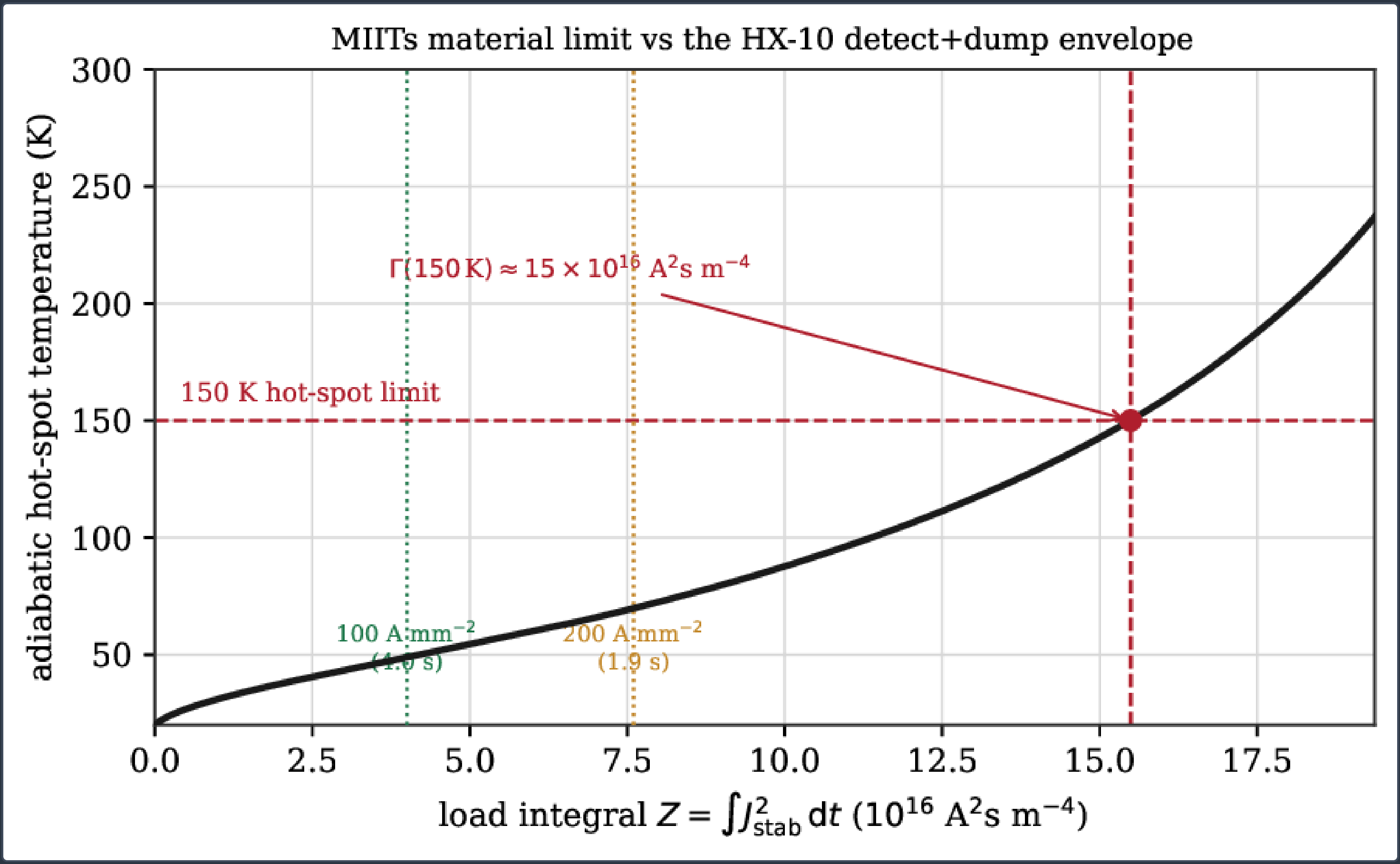

Adiabatic hot-spot (MIITs) material limit for the copper-stabilized composite (RRR ≈ 100; equation 10). Temperature reached versus load integral $Z = \int J_{\mathrm{stab}}^2 \mathrm{d}t$; the $150\,\mathrm{K}$ limit corresponds to $\Gamma(150\,\mathrm{K}) \approx 1.5 \times 10^{17}\,\mathrm{A}^2\,\mathrm{s}\,\mathrm{m}^{-4}$. Vertical markers: the HX-10 detect-and-dump operating points, both inside the limit.

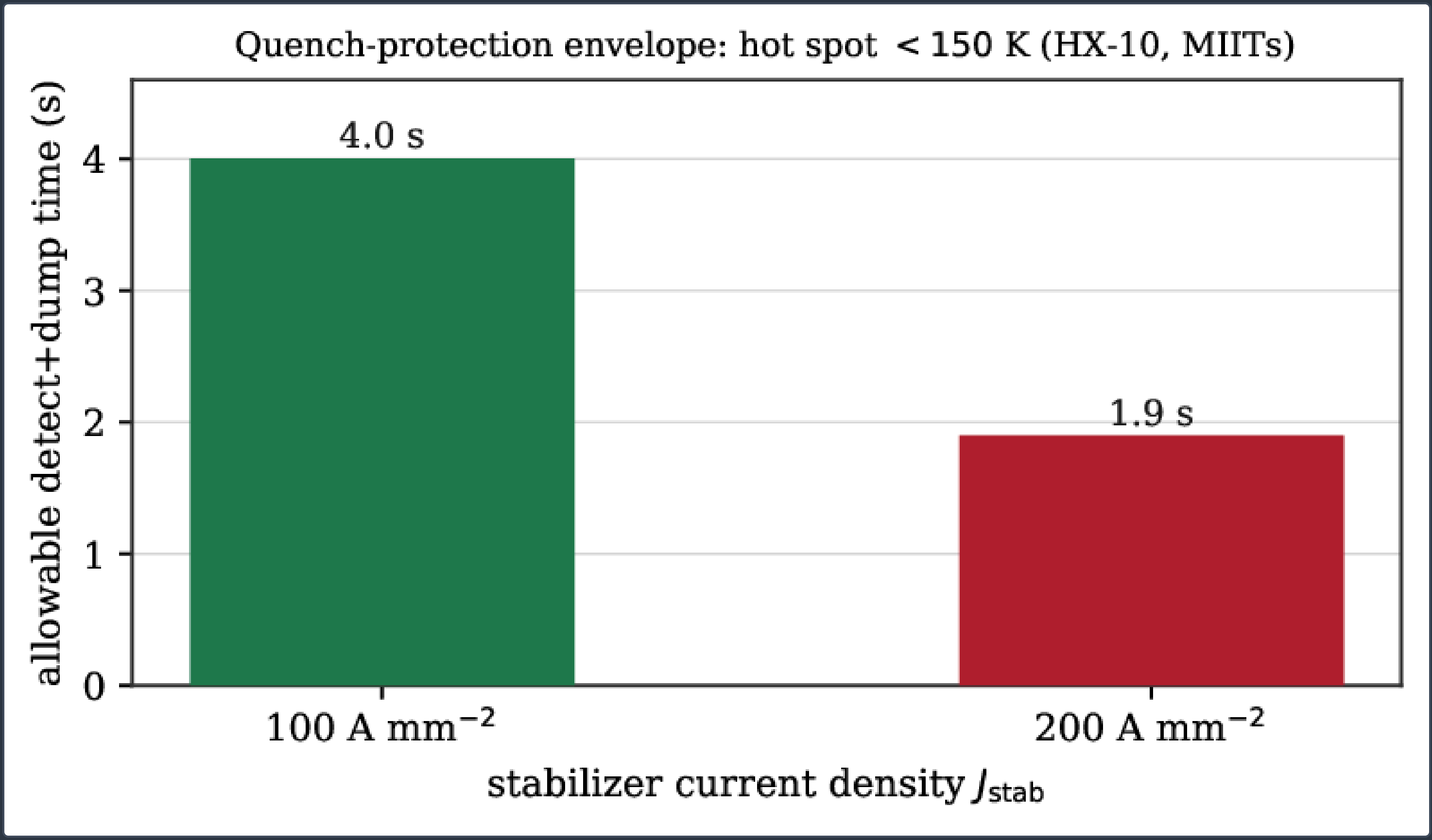

Quench-protection envelope (HX-10). Allowable detect-and-dump time to keep the adiabatic hot spot below 150 K, at two stabilizer current densities. The envelope is sized for the plug coil and lies inside the material limit of figure 5.

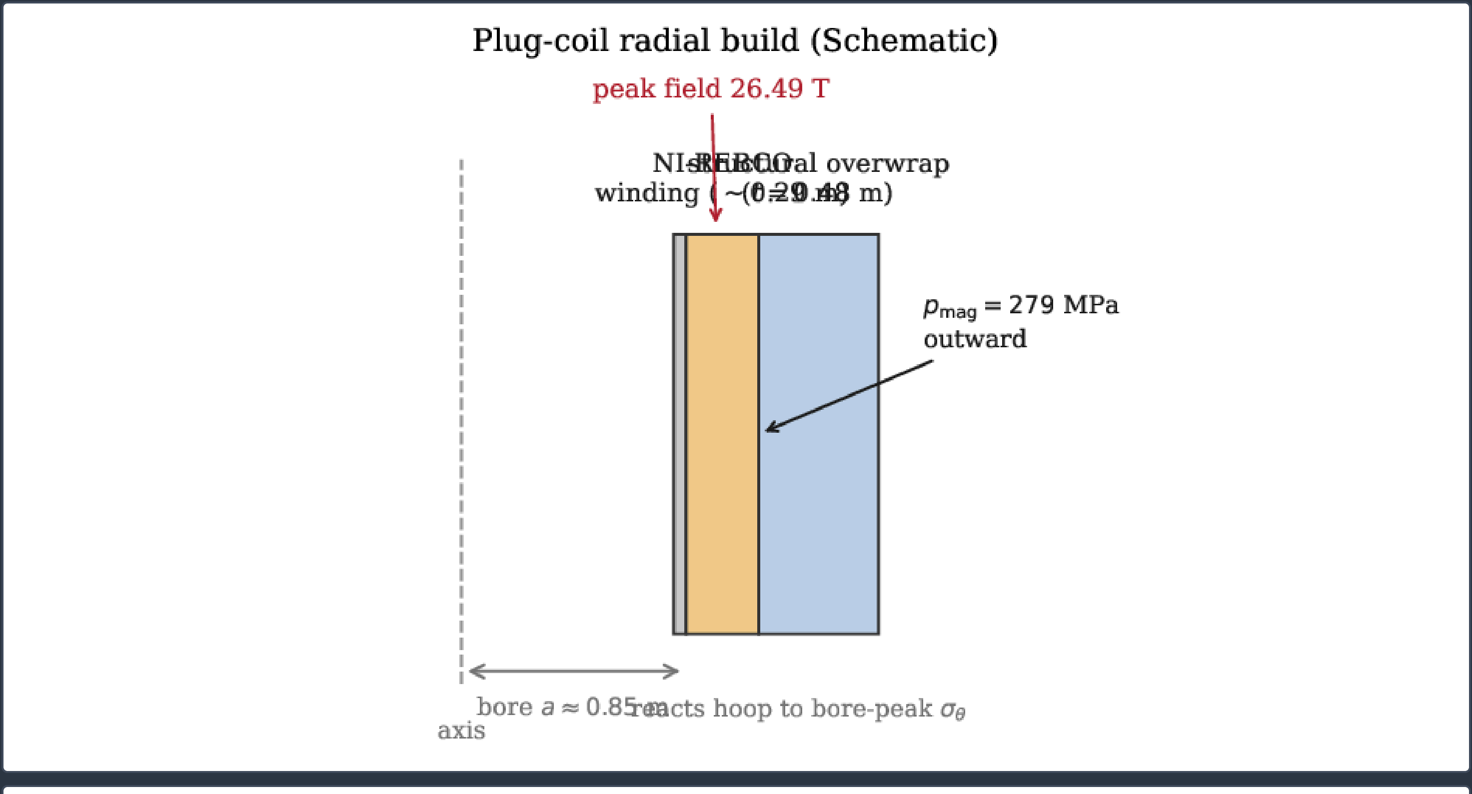

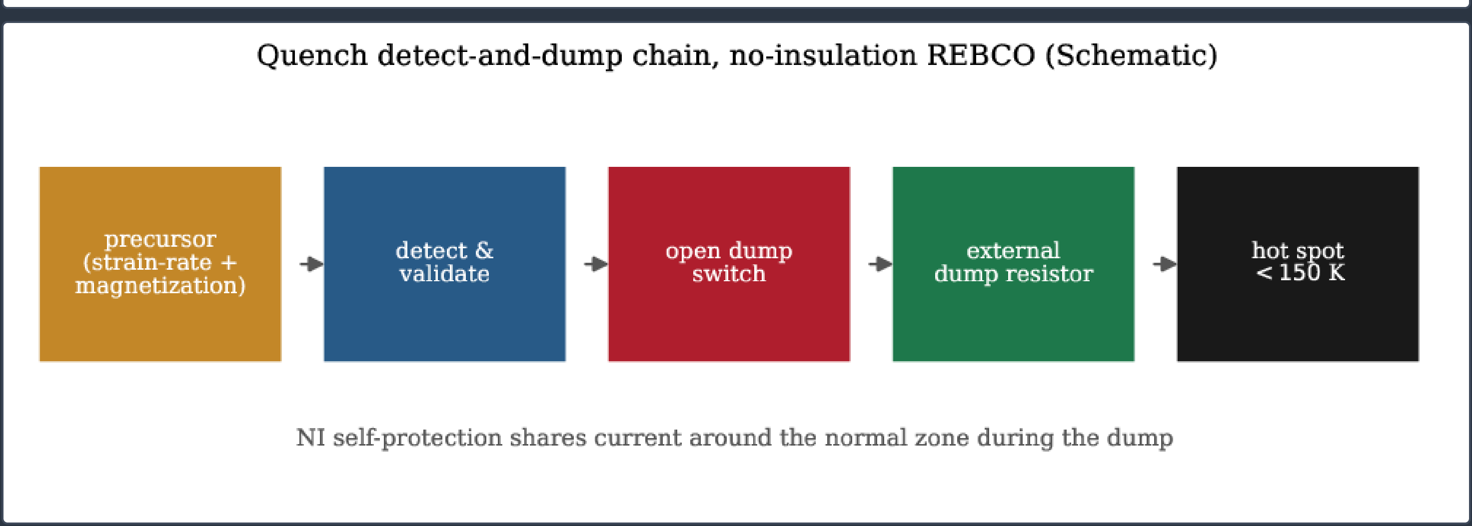

(Schematic.) Plug-coil radial build: bore ($a \approx 0.85$ m), NI-REBCO winding pack ($w \approx 0.29$ m) and structural overwrap ($t = 0.48$ m) reacting the 279 MPa magnetic pressure to a bore-peak hoop stress. No data values are plotted.

QUALIFICATION SUMMARY

Table 2 and figure 8 collect the qualification gates. The structural shell passes at a 0.66 utilization; the conductor hoop margin closes to 1.34×; the REBCO strain margin is 2.85–3.54×; the 17 T throat is comfortable; and the quench detect-and-dump envelope keeps the hot spot below 150 K within a multi-second dump. The single open item is a dedicated overfield structural-shell confirmation at +20% field (§6).

GATE	RESULT	VERDICT
structural shell, three-dimensional FE (BU-L1-A2)	440 MPa peak, 0.66 utilization vs 667 MPa	PASS
conductor hoop, real-CAD FE (AG-CX-26→P3-FEA-10)	0.86× → 1.34× margin	PASS
REBCO strain, graded preload (P3-FEA-10)	2.85–3.54× margin	PASS
17 T mirror throat (AG-CX-26)	comfortable, non-binding	PASS
quench detect+dump, MIITs (HX-10)	1.9–4 s envelope, < 150 K	PASS
overfield shell +20% (BV-09)	confirming run set up	OPEN

Plug-coil (26.49 T) qualification gates and verdicts. Serials refer to the de-risking register [30].

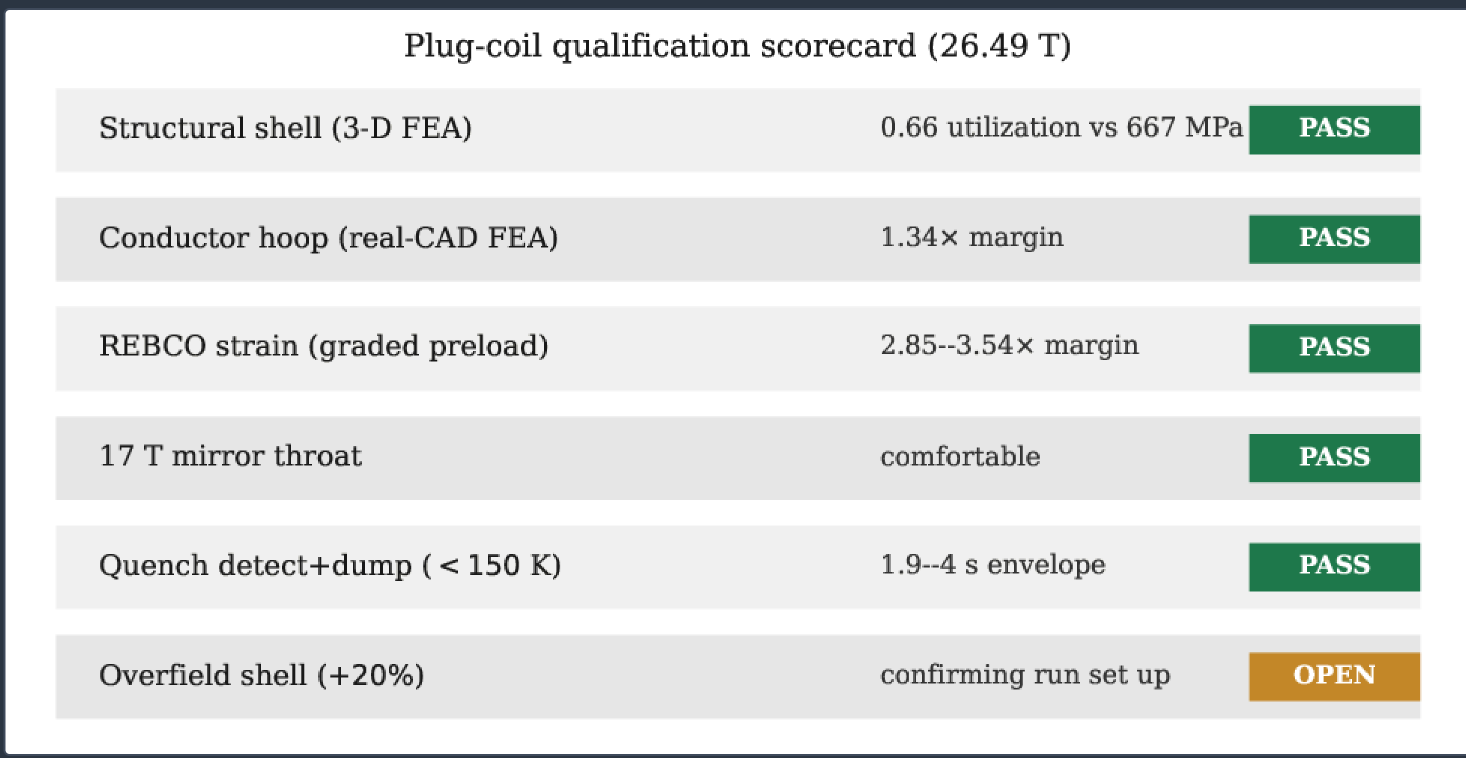

Plug-coil qualification scorecard at 26.49 T. Every structural and protection gate passes with margin; the single open item is the overfield shell confirmation (BV-09).

§ 5

Discussion

AGAINST THE HIGH-FIELD-MAGNET LITERATURE

The plug coil is a $26.49\,\mathrm{T}$ REBCO magnet, and its structural numbers should be read against the fields the community has demonstrated. The $45.5\,\mathrm{T}$ REBCO-insert record [1] and the $32\,\mathrm{T}$ all-superconducting user magnet [2] both operate above the plug's peak field, so the conductor and the field regime are not the frontier; the engineering question is the mechanical and protection design at fusion scale, which the SPARC toroidal-field model-coil program addressed for a REBCO magnet at reactor relevance [9,8]. The plug's $279\,\mathrm{MPa}$ magnetic pressure and $667\,\mathrm{MPa}$ structural allowable are conventional for high-field superconducting magnet structures [11,12], and the reconciling FE utilization of 0.66 leaves the $1.5\times$ margin that magnet practice expects. The conductor hoop-stress closure is the substantive result: coated-conductor tapes tolerate large axial stress but are strain- and delamination-sensitive [17,4], so the move from the $0.86\times$ thin-wall screen to the $1.34\times$ real-CAD margin — with a 2.85–$3.54\times$ strain margin under graded preload — is exactly the kind of load-sharing and preload engineering that qualifies a REBCO insert. The message is not that the plug reaches a record field; it is that at a field the community has already exceeded, the Kronos plug is engineered to margin in structure, conductor stress and strain simultaneously.

AGAINST THE QUENCH-PROTECTION LITERATURE

The protection case rests on the slow-NZPV physics of no-insulation REBCO. Marchevsky's review makes the core point quantitatively: in HTS conductors the large temperature margin and slow propagation mean a hot spot can reach damaging temperature before a measurable resistive voltage appears, so voltage detection alone is inadequate [14]. The community response has been non-voltage observables — fibre-Bragg thermometry demonstrated on VIPER cable at SULTAN [15] and current-distribution monitoring on fusion cables [16]. The plug's MIITs envelope (equation 11) is consistent with this picture: the $1.5 \times 10^{17}\,\mathrm{A^2\,s\,m^{-4}}$ material limit gives multi-second detect-and-dump headroom at 100–$200\,\mathrm{A\,mm^{-2}}$, comfortably longer than the microsecond-to-second response times those non-voltage detectors report, so the binding constraint is architectural rather than thermal. Matching the plug to the fused in-winding precursor demonstrated for the Kronos NI-REBCO magnets [34] closes the loop: a detector whose lead time is set by the millisecond NZPV crossing fits inside a multi-second dump envelope with room to spare.

WHY THE SEPARATION OF THE TWO MAGNETS MATTERS

Keeping the plug ($26.49\,\mathrm{T}$) and centrepost ($16.84\,\mathrm{T}$) on separate load lines (figure 4) is not bookkeeping. The two magnets differ in peak field by more than $9\,\mathrm{T}$, in load fraction (0.43 vs 0.27), and in temperature margin (37.1 vs $49.5\,\mathrm{K}$), and they belong to two different products — the tandem-mirror burner and the spherical-tokamak breeder [32,31]. Conflating their fields would either over-design the centrepost or, more dangerously, under-design the plug. The magnet-integrity case requires that each be qualified on its own critical surface, which is what this paper and its companions do.

§ 6

Limitations

One honest gate remains. The reconciling and real-CAD FE analyses qualify the coil at the **26.49 T** design point, but a dedicated three-dimensional structural-shell check at **+20%** overfield — the standard proof-margin bound — is the one confirming analysis still to run. It is set up as an `sfepy` three-dimensional model (BV-09) and is the overfield bound on the qualified design; the structural headroom already demonstrated to **30 T** (figure 1) makes it a confirmation rather than an open risk, but it is not yet a frozen result and is reported as such.

§ 7

Conclusion

The Kronos burner plug coil is a qualified **26.49 T** no-insulation REBCO magnet. Its structure carries the **279 MPa** Maxwell magnetic pressure at a **0.66** utilization of the **667 MPa** allowable, with a thick-wall Lam\'e overwrap of **0.48** m at a **0.85** m bore and demonstrated headroom to **30 T**; the conductor hoop-stress margin, **0.86**× on a conservative thin-wall screen, closes to **1.34**× on the real CAD, with a **2.85–3.54**× REBCO strain margin under a graded preload and unchanged plug dimensions; and an adiabatic hot-spot analysis places a **1.9–4** s detect-and-dump envelope, keeping the hot spot below **150** K, comfortably inside a $1.5 \times 10^{17}\ \mathrm{A^2\,s\,m^{-4}}$ material limit. The **17 T** mirror throat is never binding, and the burner plug (**26.49 T**), kept distinct from the breeder centrepost (**16.84 T**) throughout, is a structurally sound, protectable, buildable high-field magnet. Because the magnet that sets the plug density ratio is the pacing subsystem of the burner, its qualification is a load-bearing step toward the D–^{3}He tandem-mirror product [37,36,35].

Acknowledgments tocsectionAcknowledgments Part of the Kronos Fusion Energy 2026 design series. The authors thank the Kronos physics de-risking programme for the frozen result set underlying every quantitative claim, and acknowledge the NVIDIA Inception program for GPU-HPC access.

Reproducibility. The structural loads, the thick-wall Lam\'e sizing, the reconciling and real-CAD finite-element analyses, and the quench envelope are frozen anchors (BU-L1-A2, AG-CX-26, P3-FEA-10, HX-10, HX-11, SC-BU-1, KX-L1-A15) in the Kronos Physics De-Risking Register and are regenerable from the analytic, CalculiX and MIITs scripts archived with this paper. This paper is archived at doi:10.5281/zenodo.22645915; official version: https://www.kronosfusionenergy.com/publications/engineering-the-26-49-t-plug-coil-of-a-d-he-tandem-mirr.html, and the register at doi:10.5281/zenodo.22133057.

Data availability tocsectionData availability This paper is archived at doi:10.5281/zenodo.22645915. The structural tables, finite-element outputs, conductor critical-surface load lines, and quench envelope are archived with the deposit and reference the Kronos 2026 series. The figure-generation script that produced every data figure is deposited with the manuscript. Any economic analysis is reported separately and is not included in the public deposit.

Competing interests tocsectionCompeting interests Provisional patent applications relating to aspects of this work have been filed.

tocsectionReferences

APPARATUS

Portfolio, People & Record

The intellectual-property estate, the people who built it, the limitations that gate it, and the sources it rests on.

1	4	40	27
GRANTED PATENT	2026 PROVISIONALS	TEAM MEMBERS	2022 PROVISIONALS

INTELLECTUAL PROPERTY

The patent portfolio

The estate spans a granted high-field magnet patent, pending utility and 2026 provisional filings that map to the two products, a digital-twin control provisional, a registered trademark application, and the original 2022 provisional family. Every patentable disclosure in the five-paper arXiv drop was protected **before** publication: the breeder and burner provisionals were filed 1–2 August, and a publication-gap omnibus filing the evening before the drop swept up the DEC, plasma-control, and REBCO-winding matter of the three otherwise-unprotected papers. Patent numbers and application serials are matters of public record; claim scope is summarised, not reproduced.

GRANTED & PENDING UTILITY

US 12,009,112	High-field tilted graded-REBCO magnet architecture (KRONO-002A) · *app. 17/878,550*	GRANTED
US 17/878,507	Core device / method (KRONO-001A) · *utility*	PENDING

2026 PROVISIONAL FILINGS — MAPPED TO THE PRODUCTS

64/124,209	Hyperion — spherical-tokamak tritium / helium-3 foundry · *breeder · filed Aug 2026*	FILED
64/124,220	Aegis / MetroVolt — synchrotron-cutoff, fuel-selection & plug-winding · *generator · filed Aug 2026*	FILED
64/115,167	KRONOS-CTRL digital-twin plant control · *provisional · filed Jul 2026*	FILED
64/005,440	Integrated spherical-tokamak fusion architecture · *early integrated-architecture filing · filed Mar 2026*	FILED
64/105,530	Negative-triangularity spherical-tokamak architecture · *foundational ST filing · filed Jul 2026*	FILED
64/128,097	Publication-gap omnibus — quasineutral two-species expander DEC · provenance-gated / latency-split plasma control · as-built high-field winding & conductor architecture · *filed 7 Aug 2026, the evening before the arXiv drop*	FILED

TRADEMARK & ORIGIN

FTK-98801894	Kronos Fusion Energy — trademark application	FILED
KR-2022-*	Original provisional family (KR-2022-00001 … 00027) · *27 filings, 2022*	PRIORITY

The narrow, defensible magnet novelty — the specific conductor and the digital-twin winding optimisation, not high-field REBCO as a category — is the commercial core that can earn ahead of any Q > 1 milestone, with markets in fusion magnet supply, MRI/NMR, accelerators, and proton therapy. The claim is scoped honestly: the high field is a *system field* result, not a stand-alone-coil record; the small-bore plug coil is structurally infeasible as a bare winding but resolved by a stress-managed structural shield (feasible-pending-FEA); and the winding-tape experiment returned a *null result*. The value is the method, not a field record.

THE TEAM

Founding partners, board, advisors & auditors

Kronos is built by a bench of advanced-fuel-fusion, high-field-magnet, direct-conversion, and materials specialists, with a board and operations team drawn from defense, national laboratories, and industry. Dates are shown as ranges; where a tenure has ended or is term-ending, the range says so.

FOUNDING PARTNERS — SCIENCE

Dr. Gerald Kulcinski
Co-Founder · Helium-3 & Advanced-Fuel Fusion
UW–Madison · 2023–Present

Dr. Carl Weggel
Chief Scientist / S.M.A.R.T. Design
MIT Alcator Program · 2022–Present

Dr. Robert J. Weggel
Magnetic Field Design
MIT Magnet Lab · 2022–Present

BOARD

Priyanca Ford
Founder & CEO · Executive Board
2022–Present

Bandel Carano
Finance / Strategy
Oak Investment Partners / Stanford · 2025–2026

Patrick Schweiger
Fusion Device Engineering
Oklo / CFS / TerraPower · 2025–Present

SCIENTIFIC ADVISORS

Dr. Steven O. Dean
Fusion Policy & History
DOE / Fusion Power Associates · 2025–Present

Dr. Patrick H. Diamond
Plasma Turbulence & Transport
UC San Diego · 2025–Present

Dr. Jack J. Dongarra
HPC & Numerical Algorithms
Turing Award · 2025–Present

Dr. Nasr M. Ghoniem
Chief Material Scientist
UCLA · 2025–Present

Dr. Siegfried Glenzer
Plasma Physics & Laser Fusion
Stanford / SLAC · 2022–Present

Dr. David A. Hammer
Pulsed-Power Fusion
Cornell · 2025–Present

Dr. Donald A. Spong
Plasma Theory & Confinement
ORNL · 2025–Present

Dr. Curtis Smith
Risk Assessment & Nuclear PRA
MIT / Idaho National Lab · 2025–Present

RADM (Ret.) David Goggins
Naval Engineering & Power-Plant Design
U.S. Navy · 2023–2026

Dr. Konstantin Batygin
Mathematician
Caltech · 2022–2025

Dr. Ruben Fair
Magnet Design / ITER Liaison
PPPL / Jefferson Lab · 2022–2025

Dr. Paul S. Weiss
Materials & Nanotechnology
UCLA · 2022–2025

SCIENTIFIC AUDITORS

Dr. Wilfred A. Cooper
Plasma Equilibrium Theory
EPFL / Swiss Plasma Center · 2025–Present

Dr. Ahmed Hassanein
Plasma–Material Interactions
Purdue / Argonne · 2025–Present

Dr. Patrick E. Hopkins
Extreme Thermal Materials
U. of Virginia · 2025–Present

Dr. Peter Hosemann
Materials Joining & Structural Integrity
UC Berkeley · 2025–Present

Dr. Travis W. Knight
Advanced Nuclear Fuels & Systems
U. of South Carolina · 2025–Present

Dr. Philippe Lebrun
Cryogenics & Magnet Cooling
CERN · 2025–Present

Dr. Nitendra Singh
Nuclear Safety & Fuel Cycle
ITER · 2025–Present

Dr. Guido Van Oost
Magnetic Confinement & Fusion Systems
Ghent University · 2025–Present

Dr. Gary S. Was
Radiation Materials & Structural Integrity
U. of Michigan · 2025–Present

Dr. Ray Sedwick
Direct Energy Conversion
U. of Maryland · 2025

OPERATIONS

Michael Laughlin
Chief Operating Officer
2022–Present

Martin Owens
Chief Strategy Officer
LANL / GE Hitachi · 2022–Present

MG (Ret.) Paul Pardew
Chief Contracting Officer
Army Contracting Command · 2022–Present

David Beck
Fusion Commercialization
U.S. Space Force · 2024–Present

Sushma Bhatia
Environmental & Legislative
Google · 2022–Present

Michael De Frenza
Technology Licensing
2023–Present

MG (Ret.) Robin L. Fontes
Cybersecurity & Defense
Army Cyber Command · 2022–Present

Vijay Gehani
Supply Chain & Components
INOX India · 2024–Present

Jon Michel Greenwood
IT & AI Infrastructure
Live Nation · 2023–Present

Brian C. O'Neill
National Security
CIA / ODNI · 2022–Present

Gen. (Ret.) Gustave F. Perna
DoD Liaison
Operation Warp Speed · 2022–2023

Andrea Romero
Marketing Lead
2022–Present

Legal counsel is retained; those roles are held on the internal roster and are not listed here.

SOURCES

References

1 S Hahn *et al*, 45.5-tesla direct-current magnetic field generated with a high-temperature superconducting magnet, *Nature* **570** 496 (2019). doi:10.1038/s41586-019-1293-1

2 M D Bird, S Bole, I R Dixon *et al*, The NHMFL 32 T superconducting magnet: an all-superconducting user magnet with a REBCO insert, *IEEE Trans. Appl. Supercond.* **26** 4300606 (2016).

3 A Molodyk *et al*, Development and large volume production of extremely high current density $YBa_2Cu_3O_7$ superconducting wires for fusion, *Sci. Rep.* **11** 2084 (2021). doi:10.1038/s41598-021-81559-z

4 D Uglietti, A review of commercial high temperature superconducting materials for large magnets: from wires and tapes to cables and conductors, *Supercond. Sci. Technol.* **32** 053001 (2019). doi:10.1088/1361-6668/ab06a2

5 J L MacManus-Driscoll and S C Wimbush, Processing and application of high-temperature superconducting coated conductors, *Nat. Rev. Mater.* **6** 587 (2021). doi:10.1038/s41578-021-00290-3

6 S Hahn, Y Kim, D K Park, K Kim, J P Voccio, J Bascu\ n\'an and Y Iwasa, No-insulation multi-width winding technique for high temperature superconducting magnet, *Appl. Phys. Lett.* **103** 173511 (2013). doi:10.1063/1.4826217

7 B N Sorbom *et al*, ARC: a compact, high-field, fusion nuclear science facility and demonstration power plant with demountable magnets, *Fusion Eng. Des.* **100** 378 (2015). doi:10.1016/j.fusengdes.2015.07.008

8 A J Creely *et al*, Overview of the SPARC tokamak, *J. Plasma Phys.* **86** 865860502 (2020). doi:10.1017/S0022377820001257

9 Z S Hartwig *et al*, The SPARC toroidal field model coil program, *IEEE Trans. Appl. Supercond.* **34** 0600316 (2024).

10 S P Timoshenko and J N Goodier, *Theory of Elasticity*, 3rd ed. (McGraw–Hill, New York, 1970).

11 M N Wilson, *Superconducting Magnets* (Oxford University Press, Oxford, 1983).

12 Y Iwasa, *Case Studies in Superconducting Magnets: Design and Operational Issues*, 2nd ed. (Springer, New York, 2009).

13 G Dhondt, *The Finite Element Method for Three-Dimensional Thermomechanical Applications* (Wiley, Chichester, 2004); CalculiX CrunchiX (`ccx`) implicit finite-element solver.

14 M Marchevsky, Quench detection and protection for high-temperature superconductor accelerator magnets, *Instruments* **5** 27 (2021). doi:10.3390/instruments5030027

15 E E Salazar *et al*, Fiber optic quench detection for large-scale HTS magnets demonstrated on VIPER cable during high-fidelity testing at the SULTAN facility, *Supercond. Sci. Technol.* **34** 035027 (2021). doi:10.1088/1361-6668/abdba8

16 R Teyber, J Weiss, M Marchevsky, S Prestemon and D van der Laan, Current distribution monitoring enables quench and damage detection in superconducting fusion magnets, *Sci. Rep.* **12** 22503 (2022). doi:10.1038/s41598-022-26592-2

17 M Sugano, K Osamura, W Prusseit, R Semerad, K Itoh and T Kiyoshi, Tensile fracture behaviour and strain dependence of critical current for YBCO coated conductors, *Supercond. Sci. Technol.* **18** S344 (2005).

18 D C van der Laan, J D Weiss and D M McRae, Status of CORC cables and wires for use in high-field magnets and power systems, *Supercond. Sci. Technol.* **32** 033001 (2019).

19 Y Yanagisawa *et al*, Effect of current sweep reversal on the magnetic field stability of a REBCO no-insulation coil, *Physica C* **471** 1177 (2011).

20 D C Larbalestier *et al*, Isotropic round-wire multifilament cuprate superconductor for generation of magnetic fields above 30 T, *Nat. Mater.* **13** 375 (2014). doi:10.1038/nmat3887

21 J W Ekin, *Experimental Techniques for Low-Temperature Measurements* (Oxford University Press, Oxford, 2006).

22 J E Menard *et al*, Fusion nuclear science facilities and pilot plants based on the spherical tokamak, *Nucl. Fusion* **56** 106023 (2016). doi:10.1088/0029-5515/56/10/106023

23 R F Post, The magnetic mirror approach to fusion, *Nucl. Fusion* **27** 1579 (1987).

24 T K Fowler, R W Moir and T C Simonen, A new simpler way to obtain high fusion power gain in tandem mirrors, *Nucl. Fusion* **57**

COLOPHON

How this document was made

The Kronos Fleet — Combined Editorial, 2026 is set in **Fraunces** (display), **Gelasio** (text), and **IBM Plex Mono** (data & equations), carried forward from the Kronos editorial design system.

The figures are rendered at 300 dpi from the deposited generator scripts; the document is composed as a single self-contained file with embedded fonts and imagery, paginated to US Letter, and rendered to PDF through a headless Chromium engine in matched light and dark editions.

Every headline quantity carries an evidence class; withdrawn and restated values are marked as such. Nothing herein is frozen beyond the founder-approved Tier-A set.

Explore it live — turn the interactive 3-D model, run the deposited solvers in the physics validator, and watch the companion film series.

LEGAL NOTICE

Notice, status, and distribution

Conceptual design & simulation study. This document reports a conceptual design and simulation study. It is not a construction commitment, a safety-analysis report, a regulatory filing, or an offer of securities. Forward-looking statements — schedules, costs, market sizes, and performance — are estimates subject to the limitations set out in the Simulations part and may change.

Numbers and their classes. Quantities are reported with evidence classes and case labels; modelled, assumed, and requirement-class values are identified as such and are not to be quoted without their labels.

Public edition. This edition carries the physics and design only; all financial, funding, and defense-commercial content has been removed for public distribution. The scientific text corresponds to the arXiv and journal submissions.

THE 2026 KRONOS SERIES

One programme, many papers

This editorial is one paper in the Kronos 2026 series — a real fusion company's complete, reproducible physics record for a spherical-tokamak breeder and its low-neutron D–^{3}He tandem-mirror burners. Every headline number is a frozen anchor in the Physics De-Risking Register.

Explore the whole programme: the De-Risking Register, the interactive 3-D model, and the physics validator.

KRONOS FUSION ENERGY

Engineering the 26.49 T Plug Coil of a D–^{3}He Tandem-Mirror Burner: Three-Dimensional Structural FEA, No-Insulation REBCO Quench Margin and Throat-Conductor Stress

A real fusion company building real machines. Explore the science, live.

Zenodo · doi:10.5281/zenodo.22645915

Read on kronosfusionenergy.com

The Physics De-Risking Register